

Nanoconfined catalytic Ångström-size motors

Peter H. Colberg^a and Raymond Kapral^{*a}

Received Xth XXXXXXXXXX 20XX, Accepted Xth XXXXXXXXXX 20XX

First published on the web Xth XXXXXXXXXX 200X

DOI: 10.1039/b000000x

Chemically-powered synthetic micron and nano-scale motors that propel themselves in solution are being intensively studied because of the wide range of potential applications that exploit their directed motion. Recent experiments have shown that, even on the molecular scale, small-molecule catalysts and single enzyme molecules exhibit properties that have been attributed to self-propulsion. Simulations of very small Ångström-size synthetic motors in bulk solution have shown similar effects. Applications of such small motors in the cell or in microfluidic devices require knowledge of how these motors interact with boundaries. Molecular dynamics is used to investigate the properties of Ångström-size synthetic chemically-powered motors confined between walls separated by distances of tens of nanometers. Evidence for strong structural ordering of the motors between the walls, which reflects the finite size of solvent molecules and depends on solvent exclusion forces, is provided. Dynamical properties, such as average motor velocity, orientational relaxation and mean square displacement, are anisotropic and depend on the distance from the walls. This research presents information needed for potential applications that use these motors in the complex confined geometries encountered in biology and the laboratory.

1 Introduction

Synthetic self-propelled motors that convert chemical energy from their environment into directed motion are examples of active objects with distinctive and useful properties. Much of the interest in such motors stems from potential applications that exploit their directed motion to carry out functions involving cargo transport, analogous to the active transport tasks performed by molecular motors in the cell.^{1–4} Self-diffusiophoresis is one mechanism that chemically-powered motors use to produce motion from chemical energy.^{5–8} In this mechanism, a chemical reaction on a portion of the motor leads to asymmetric distributions of reactants and products in the motor vicinity, which give rise to a force on the motor that is responsible for its directed motion.

In many circumstances motors operate in complex environments or systems confined by boundaries. Examples include motors used in microfluidic devices⁹ and potential *in vivo* applications such as targeted drug delivery^{10,11}. Also, in many experiments currently being carried out, motors reside near a surface as a result of gravitational or other forces, and the interactions of motors with surfaces can lead to interesting dynamical effects.^{12–15} For these reasons it is important to assess the influence of boundaries and confinement on motor dynamics.

The effects of confinement on motor motion have been investigated previously. The velocity of a spherical self-

propelled particle with a point-like catalytic site confined by a spherical wall has been computed analytically.¹⁶ Micron-scale Janus motors operating by self-diffusiophoresis have been studied experimentally and numerically in circumstances where they collide with a wall, are confined to a circular pore, and move through a triangular lattice of obstacles forming a patterned environment.¹⁷ The dynamics of a self-diffusiophoretic Janus particle close to a hard wall has been shown to exhibit reflection, steady sliding, and hovering.¹⁸ A study of such Janus particles near a wall has been carried out using continuum hydrodynamics.¹⁹ The rectification of a Brownian Janus particle in a triangular channel²⁰ and the escape of an ellipsoidal Brownian Janus particle from a two-dimensional sinusoidally corrugated or square-shaped pore have been simulated.²¹ The accumulation of self-propelled Brownian spheres near a hard wall has been studied analytically and simulated using multi-particle collision dynamics.²²

In a related but somewhat different context, the effects of hydrodynamic interactions on the confined motions of swimmers and biological organisms have also been investigated. Since biological organisms function in environments containing obstacles and boundaries of various types, such studies are essential in order to obtain a full understanding of swimming motions in a biological context. Studies of hydrodynamic effects on self-propulsion of both synthetic swimmers and biological organisms near boundaries and in complex media have been carried out.^{23–27} Boundaries can influence the collective behavior of swimmers and the collective motions of swimmers confined to the gap between two planar surfaces have been ob-

^a Chemical Physics Theory Group, Department of Chemistry, University of Toronto, Toronto, Ontario M5S 3H6, Canada. E-mail: rkapral@chem.utoronto.ca

served.^{25,26}

Several factors must be considered in order to understand the effects of confinement on chemically-powered motors. These include: direct interactions with the boundaries, motor geometry, the influence of boundaries on hydrodynamic flows and the nature of chemical gradients near walls. At the micron to nanometer scales self-propulsion is influenced by thermal fluctuations. Orientational Brownian motion limits the duration of the ballistic regime where directed motion can be observed and leads to diffusive dynamics on long time scales, albeit characterized by diffusion coefficients that reflect the underlying active motion. Interactions with boundaries can influence orientational Brownian motion and modify motor behavior.

In this paper we consider a regime of motor dynamics and confinement that differs from that in earlier investigations. We focus on very small Ångström-scale motors confined in thin nanometer-scale layers between two walls. This study is prompted by several observations. Recent experiments have demonstrated that catalytically active 5 Å organometallic molecules²⁸ as well as single enzyme molecules^{29,30} display enhanced diffusion compared to the same systems in the absence of chemical activity. In addition, experimental studies of very small (30 nm) synthetic self-propelled Janus particles have also found enhanced diffusion coefficients³¹. Although the precise mechanism responsible for diffusion enhancement is still a matter of debate for the molecular systems, self-propulsion on the Ångström scale provides a possible explanation for these observations. Such enzymatically induced motion has been reviewed recently.³² In addition to these experimental results, molecular dynamics simulations of chemically propelled Ångström-size sphere-dimer motors that operate by self-diffusiophoresis have shown that these motors can move distances of one to several times their length before they reorient and have enhanced diffusion coefficients.³³

For such small-scale motors, whose size is comparable to the molecules comprising the environment, solvent structural effects play an important role and fluctuations dominate their behavior. Nevertheless, the signatures of self-propulsion are clearly evident in observable properties such as diffusion coefficients. Enzymes carry out their functions in the complex cellular environment and, potentially, very small synthetic motors will find applications on the cellular level and other confined systems. It is then important to consider effects due to the confinement on these very small motors.

The outline of the paper is as follows: In Sec. 2 we describe the model for the motor and solvent molecules, along with their interactions with the walls that confine them. Section 3 presents results on static structural properties, in particular, the nature of the motor position and its angular distributions perpendicular and parallel to the walls. Dynamical properties, including dimer velocity, orientational correlations, and mean

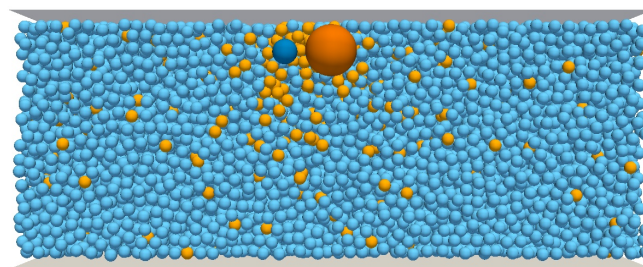


Fig. 1 Cross section of sphere-dimer motor with spheres C (blue) and N (vermillion) immersed in A (sky blue) and B (orange) solvent particles confined between two planar walls a distance $L_Z = 20$ apart.

square displacement, are discussed in Sec. 4. The conclusions of the study are given in Sec. 5.

2 Confined self-propelled motors

We consider a self-propelled Ångström-scale motor confined between two parallel walls. The specific chemically-powered motor we study is a sphere-dimer that consists of linked catalytic and noncatalytic spheres and operates through a diffusiophoretic mechanism.³⁴ Experimental¹⁴ and simulation^{35,36} studies of the motions of these motors in bulk solution have been carried out. Motor geometry is a factor to consider when dealing with wall interactions, and sphere-dimer motors are simple examples of more complex, non-spherical motors. They also capture some important features of molecular motors, namely non-spherical shapes and localized chemically active sites.

In more detail, the sphere-dimer motor we consider consists of a catalytic C sphere and a noncatalytic N sphere, with diameters $\sigma_C = 2\sigma$ and $\sigma_N = 4\sigma$, respectively, linked by a rigid bond of length d . The solvent consists of N_s structureless A and B particles with diameter σ and mass m . The solvent number density is $\rho_s = N_s/V = 0.8\sigma^{-3}$, which corresponds to a dense fluid. The sphere dimer masses, $M_m = \frac{\pi}{6}\rho_s m(\sigma_C^3 + \sigma_N^3)$, are chosen to make the dimer neutrally buoyant. All particles interact through a shifted, truncated Lennard-Jones potential, $V_{ij}(r) = \epsilon_{ij}(4((\sigma_{ij}/r)^{12} - (\sigma_{ij}/r)^6) + 1)$ for $r < \sqrt[6]{2}\sigma_{ij}$ and zero otherwise. Here r is the distance between the centres of a pair of particles, $\sigma_{CA} = \sigma_{CB} = \frac{1}{2}(\sigma_C + \sigma)$ and $\sigma_{NA} = \sigma_{NB} = \frac{1}{2}(\sigma_N + \sigma)$ for pairs of dimer sphere and solvent particle, and $\sigma_{AA} = \sigma_{AB} = \sigma_{BB} = \sigma$ for pairs of solvent particles. The interaction energy is ϵ for all pairs apart from NB pairs, where $\epsilon_{NB} = 0.1\epsilon$. The temperature of the system is $k_B T/\epsilon = 1$.

The system is contained in a slab with edge lengths $L_X \times L_Y \times L_Z = 20 \times 20 \times 10, 15, \dots, 50\sigma^3$ with periodic boundary conditions in X and Y directions and two planar walls at

$Z = 0$ and L_Z . The dimer spheres and solvent particles interact with the walls via a repulsive 9-3 Lennard-Jones potential, $V_S(\zeta) = (3\sqrt{3}/2)\epsilon_{wS}((\sigma_{wS}/\zeta)^9 - (\sigma_{wS}/\zeta)^3 + 1)$ for $\zeta < 3^{1/6}\sigma_{wS}$, where ζ is the distance to the closest wall, and zero otherwise. The wall interaction parameters are $\sigma_{wA} = \sigma_{wB} = 1$, $\sigma_{wC} = (\sigma_C + 1)/2$, $\sigma_{wN} = (\sigma_N + 1)/2$, and $\epsilon_{wA} = \epsilon_{wB} = \epsilon_{wC} = \epsilon_{wN} = 1$.

The C sphere catalyses the reaction $A \rightarrow B$, where A is converted to B with unit probability when it lies within a distance $\sqrt[3]{2}\sigma_{CB}$ from the C sphere. The system is maintained in a nonequilibrium steady state through a bulk back-reaction $B \rightarrow A$ with rate $10^{-3}\tau^{-1}$ outside of the C- and N-sphere interaction zones. The dimer bond length is taken to be $d = \sqrt[3]{2}(\sigma_{CB} + \sigma_{NB})$, which is chosen to ensure energy conservation in the presence of reactions.

Since dynamics on the Ångström scale is being studied, full molecular dynamics³⁷ is used to follow the motions of the motor and solvent. The velocity-Verlet integration timestep for the molecular dynamics simulations is $10^{-3}\tau$. Simulation results are reported in dimensionless units with distance given in units of σ , mass in units of m , energy in units of ϵ , and time in units of $\tau = \sigma\sqrt{m\epsilon}^{-1}$.

Parameters were chosen to model a dense fluid Argon-like solvent. Given Argon³⁸ values of $\sigma = 0.34\text{ nm}$, $\epsilon = 120\text{ K}k_B$, and $m = 39.95\text{ u}$ and $\tau = 2.15\text{ ps}$, we can assign physical values to our Ångström-scale motor simulations. In these units the sphere-dimer monomers have radii of 0.34 nm and 0.68 nm for the C and N spheres, respectively. The end-to-end length of the sphere-dimer motor is 2.55 nm . The separation between the walls varies from 3.4 nm to 17 nm .

An instantaneous configuration of the sphere dimer and surrounding A and B solvent species confined between two walls is shown in Fig. 1. In this figure one can see the relative sizes of dimer monomers and solvent particles, as well as the inhomogeneous distribution of reactants and products near the dimer and wall, which will play an important role in the subsequent discussion.

3 Structured ordering of dimer motor in confined geometry

We begin by considering the structural ordering of the sphere-dimer motor when it is confined between the two walls. Information on this structure was extracted from averages over many trajectories of the time evolution of the system. In order to isolate structural effects that are due to the self-propulsion of the motor, results for inactive dimers will also be presented. Inactive dimers were constructed by turning off the chemical reactions that power the motor and maintain the system in a nonequilibrium steady state.

Sample trajectories of an inactive dimer and a sphere-dimer

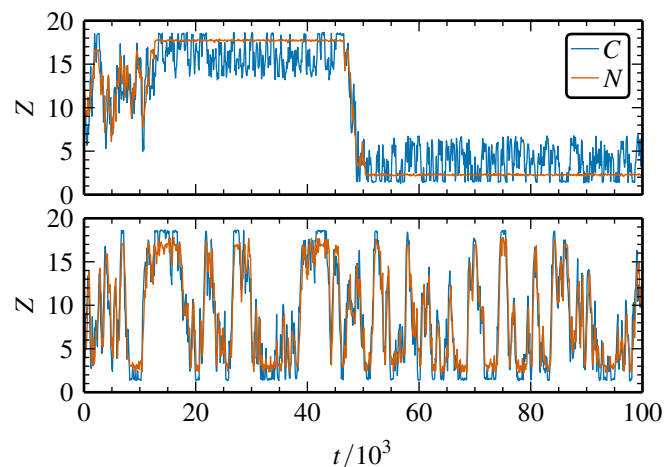


Fig. 2 Trajectories of the perpendicular distances of the N (red) and C (blue) dimer spheres to walls, Z , versus time, for an inactive dimer (top) and a sphere-dimer motor (bottom). The separation between the walls is $L_Z = 20$.

motor confined by the two walls are shown in Fig. 2. In the upper panel of this figure we see that the inactive dimer spends most of its time close to either wall with short, infrequent transitions between the walls. The larger N sphere resides primarily at a fixed distance from the wall. Solvent exclusion forces play a significant part in structural ordering and these forces are responsible for the strong effective attraction of the larger dimer monomer to the wall. The exclusion forces are weaker for the smaller C sphere and it explores a larger configuration space region, which is limited by the dimer bond constraint. By contrast, the sphere-dimer motor spends short times at either wall and frequently transitions between the walls (lower panel). Neither sphere is locked to a particular distance from the wall. Self-propulsion enables the dimer to overcome the exclusion forces that act on the spheres and confine the inactive dimer to the walls for much of the time.

The probability densities of both sphere positions for an inactive dimer and a sphere-dimer motor are shown in Fig 3. For the inactive dimer the N sphere has a pronounced peak at $\zeta = 2.2$, with negligible peaks at approximately $\zeta = 3.5, 4.5, \dots$, corresponding to separations of σ , the diameter of a solvent molecule. Far from the wall the density is uniform. The C sphere shows structural effects, too, with multiple peaks of decreasing amplitude at separation intervals corresponding to the size of a solvent molecule; however, the first peak is smaller than that of the N sphere. (The effects of the excluded volume of the solvent on the solvent density close to the walls can be seen more clearly in Fig. 4.) The density drops sharply to the same uniform distribution as for the N sphere at $\zeta = 6.7$, which corresponds to a distance $\Delta\zeta = 4.5$ equivalent to the

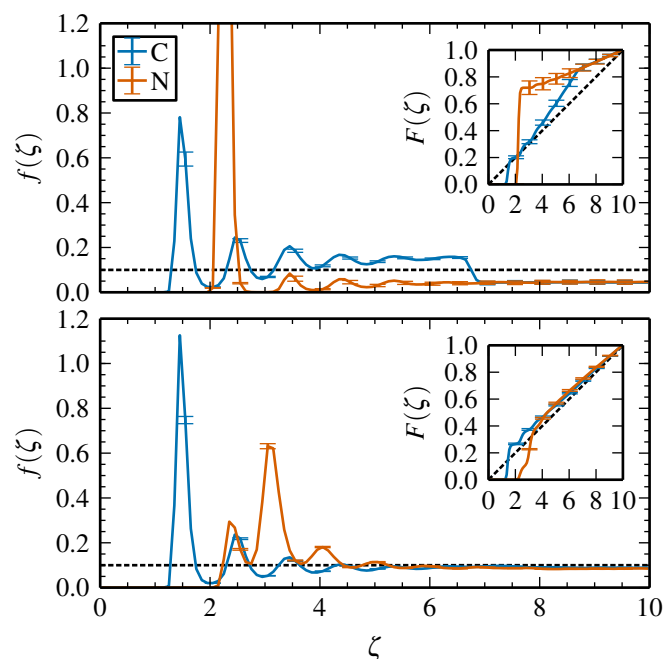


Fig. 3 Probability density $f(\zeta)$ of the distance ζ between each dimer-sphere and the nearest wall, for an inactive dimer (top) and a motor (bottom), for a wall-wall distance $L_Z = 20$. The insets show the corresponding cumulative probability density $F(\zeta)$. The dashed lines indicate uniform density distributions.

dimer bond length from the density peak of the N sphere. For the self-propelled sphere-dimer motor, the relation between the first peaks of the C and N spheres is inverted. The C sphere has the first and largest peak at $\zeta = 1.6$ with peaks of decreasing magnitude at $\zeta = 2.5, 3.5$ and 4.5 . The first peak of the N sphere is significantly smaller than its second peak. For both spheres the density converges to a uniform distribution for $\zeta > 6$.

The insets of Fig. 3 show the probability densities plotted as cumulative distributions. The N sphere is trapped at a fixed distance from the wall with a cumulative probability of 70%. For the C sphere the cumulative probability of the first peak is 20%. Both spheres exhibit densities that are far from a uniform distribution. By contrast, the cumulative probability densities show that the sphere positions of the sphere-dimer motor are close to a uniform distribution for $\zeta > 4$.

The structural ordering of the solvent also effects the average orientation of the dimer relative to the walls. We denote with \mathbf{z} the bond vector pointing along the propulsion direction from the centers of the N to C spheres, and separate the contributions perpendicular and parallel to the wall, z_{\perp} and z_{\parallel} , respectively. The probability density of z_{\parallel} assumes a uniform distribution due the periodic boundary con-

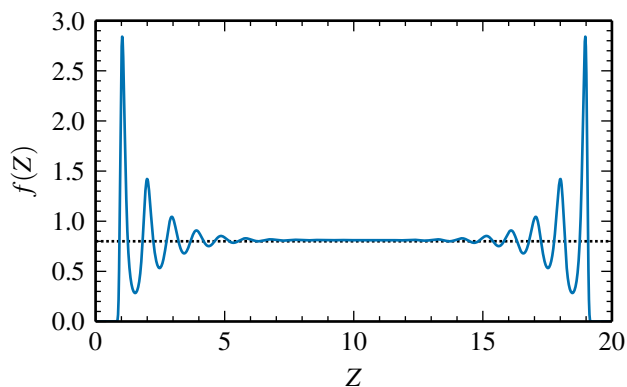


Fig. 4 Probability density $f(z)$ of solvent molecules as a function of z for $L_Z = 20$. The dotted line shows the solvent number density ρ_s . The density oscillates in manner typical of a dense fluid at a planar boundary with the largest peak at $\zeta = 1$ and subsequent peaks decreasing in amplitude at $\zeta = 2, 3$, etc.

ditions in the X and Y dimensions. The probability density of z_{\perp} is strongly nonuniform, as seen in Fig. 5 for both inactive and sphere-dimer motors. The orientation ranges from $z_{\perp} = -d \dots d = -4.5 \dots 4.5$, where $z_{\perp} = -4.5$ corresponds to the dimer being perpendicular to the wall with the C sphere oriented towards the wall, and $z_{\perp} = 4.5$ to the dimer being perpendicular to the wall with the N sphere oriented towards the wall. The probability density of the inactive dimer has a maximum at $z_{\perp} = -0.8$, which corresponds to the N and C spheres contacting the wall and is approximately equal to the difference of their potential radii with the wall, $\sigma_{wC} - \sigma_{wN} = -1$. For $z_{\perp} > -0.8$ the density oscillates with peaks of decaying intensity at $z_{\perp} = 0.2, 1.2, 2.2, \dots$, which corresponds to the N sphere locked at a fixed distance from the wall and the C sphere exploring the wall region within the confinement of the dimer bond, where the density oscillation is the signature of the solvent structure. For $z_{\perp} < -0.8$ the density shows minor peaks due to the solvent structure but is otherwise close to zero. For the sphere-dimer motor the probability density has a large peak at $z_{\perp} = -1.6$ and a smaller peak at $z_{\perp} = -0.9$. The configuration with the C sphere contacting the wall and the N sphere separated from the wall by a layer of solvent molecules thus has a higher probability than the configuration with both spheres contacting the wall. For $z_{\perp} > 0$ the density decays slowly, since, in contrast to the inactive dimer, self-propulsion allows the motor to overcome the strong solvent exclusion force on the N sphere.

The effects of confinement on suspensions of hydrodynamically interacting pusher and puller swimmers was investigated by Hernandez, et al.²⁶ The swimmers were modeled as dimers comprising beads linked by a stiff spring, subject to a force that gives rise to propulsion. Considering only very low dimer

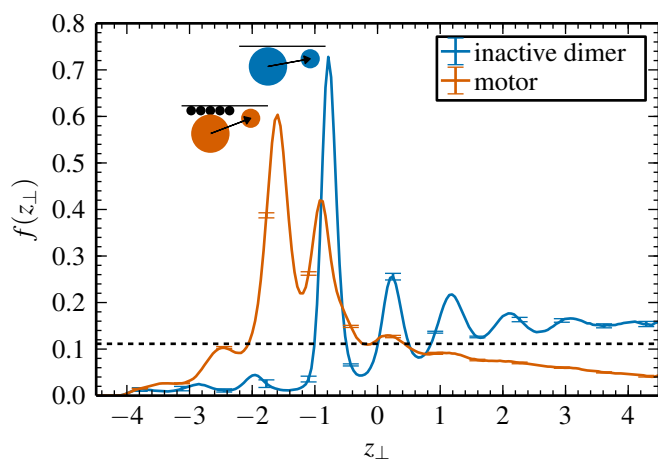


Fig. 5 Probability density $f(z_{\perp})$ of the perpendicular component of the dimer bond vector, z_{\perp} , for an inactive dimer and a sphere-dimer motor, for a wall-wall distance $L_Z = 20$. The diagrams next to the maximum peaks for the inactive dimer and motor illustrate their most likely configurations; for the motor the configuration includes a layer of solvent molecules between N sphere and wall. A positive z_{\perp} indicates that the center of the N sphere is closer to the nearest wall than the center of the C sphere, and vice versa. The probability density is averaged over the two wall regions, where the dimer is defined to be in the wall region if its center of mass is within a distance of 5 from the nearest wall. The dotted line shows a uniform distribution.

densities, the swimmer concentration profile as a function of the distance from the walls has peaks near the walls. As one moves farther from walls the concentration falls to close to zero values for pushers and to non-zero values for pullers. These findings may be compared with our single sphere dimer results. The continuum theory for sphere-dimer motors that operate by self-diffusiophoresis has been carried out.^{39,40} For small dimer bond lengths the far-field fluid flow is characteristic of a puller, while for long bond lengths it becomes a pusher.⁴⁰ Assuming such a continuum description applies to the far-field flow generated by our Ångström-size sphere-dimer motor, it would act as a puller, and our results are consistent with the hydrodynamic model. However, we note that our simulations include a variety of other effects including the self-generated chemical gradients, solvent structure and exclusion forces, fluctuations as well as hydrodynamics.

4 Motor dynamics in confined geometry

The catalytic reaction at the C sphere is responsible for a propulsion force along the dimer bond which, for our choice of interaction parameters, results in a mean motor velocity, $\langle V_z \rangle \neq 0$, directed from the N to C spheres. The motor velocity

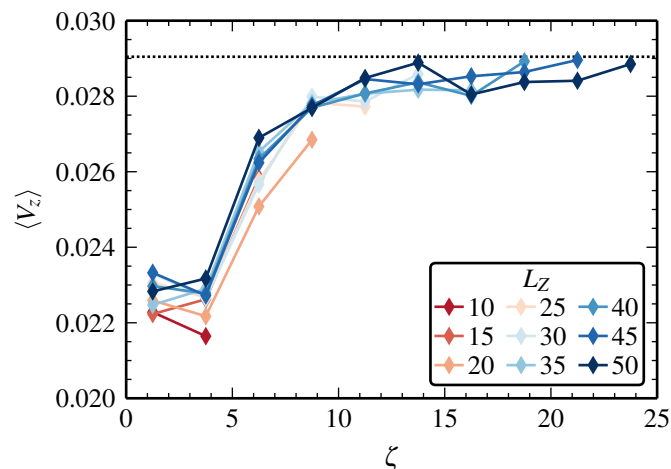


Fig. 6 Average propulsion velocity, $\langle V_z \rangle$, of a confined dimer motor as a function of the distance ζ to the closest wall. The velocities are averaged over slabs of width $\Delta Z = 5$ parallel to the walls. The dotted line shows the propulsion velocity of an unconfined dimer motor.

is shown in Fig. 6 as a function of the distance from the wall for various wall separations, L_Z . Close to the wall at $\zeta < 5$ dimer propulsion is suppressed leading to smaller mean velocities of approximately $V_z = 0.023$. Far from a wall at $\zeta > 15$ the velocity converges to the limit value $V_z = 0.029$ corresponding to that of a dimer motor without confinement. A dimer confined in a narrower slab with $L_Z \leq 20$ has a slightly smaller velocity close to the wall than a dimer confined in a wider slab, but overall the velocity profile is roughly independent of L_Z .

The dimer is subject to strong thermal fluctuations from the solvent that affect its translational and rotational motion. In particular, rotational Brownian motion will reorient the dimer motor so that its ballistic motion will only be manifest for times less than the average reorientation time. (In fact, for these Ångström-size dimer motors the ballistic regime is dominated by thermal inertial effects.³³) For times longer than this the behavior will be diffusive but with an enhanced diffusion coefficient. As discussed earlier, these reorientation effects are especially strong for Ångström-size dimers and the crossover from ballistic to diffusive motion occurs on the time scale of picoseconds. For a dimer motor confined by two parallel walls rotational motion is no longer isotropic and it is interesting to examine how confinement influences this property.

If, as earlier, we denote by $\hat{\mathbf{z}}$ the unit vector along the dimer bond, we may resolve this quantity into its components perpendicular and parallel to the wall, $\hat{\mathbf{z}}_{\perp}$ and $\hat{\mathbf{z}}_{\parallel}$, respectively. The corresponding orientational correlation functions are $C_{\perp}(t) = \langle \hat{\mathbf{z}}_{\perp}(t) \hat{\mathbf{z}}_{\perp} \rangle$ and $C_{\parallel}(t) = \langle \hat{\mathbf{z}}_{\parallel}(t) \hat{\mathbf{z}}_{\parallel} \rangle$, and are plotted in Fig. 7 versus time for both inactive dimers and dimer mo-

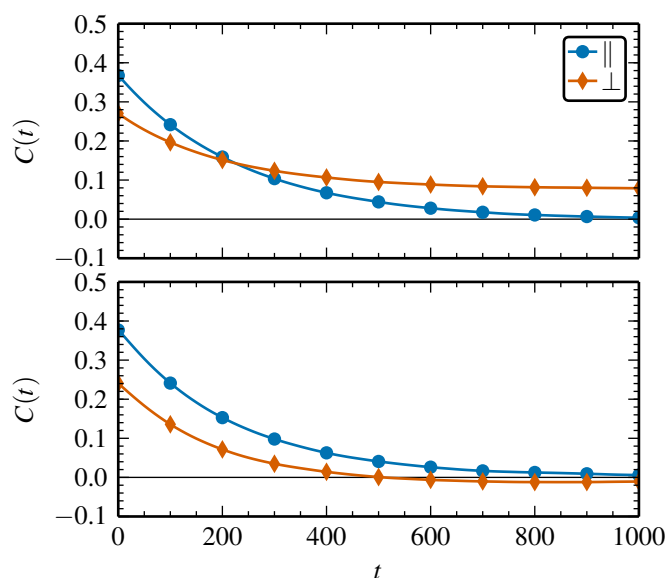


Fig. 7 Parallel (\parallel) and perpendicular (\perp) orientational autocorrelation function of a confined inactive dimer (top) and a confined sphere-dimer motor (bottom) for a wall-wall distance $L_Z = 20$.

tors. The autocorrelation functions of the parallel components are essentially the same for both inactive dimers and sphere-dimer motors and decay to zero. By contrast, the autocorrelation of the perpendicular components behave differently. This correlation function decays more slowly and to a non-zero value for the inactive dimer, consistent with the observation that inactive dimers tend to be trapped at the walls by strong exclusion forces. Also, in this configuration the motor makes an angle with the wall because of the different sphere monomer sizes. The dimer motor is not locked to the wall, its orientational autocorrelation function decays to zero, and it decays more rapidly due to interactions with the wall that lead to reorientation.

The orientational relaxation times τ_r extracted from such autocorrelation plots are shown in Fig. 8 as a function of the separation L_Z between the walls. The most notable feature of these plots is the fact that for the dimer motor τ_r for the perpendicular component increases to a shallow maximum and then tends to a smaller constant value as L_Z increases. By contrast, the relaxation time for the parallel component simply slowly decays as L_Z increases. The inactive dimer results are qualitatively similar but show much less pronounced trends.

As discussed earlier, one of the major, easily-obtainable signature of propulsion for very small motors is the existence of enhanced diffusion. Confinement will influence this transport property. We have shown earlier³³ that the mean square displacement (MSD) of an unconfined Ångström-scale sphere-

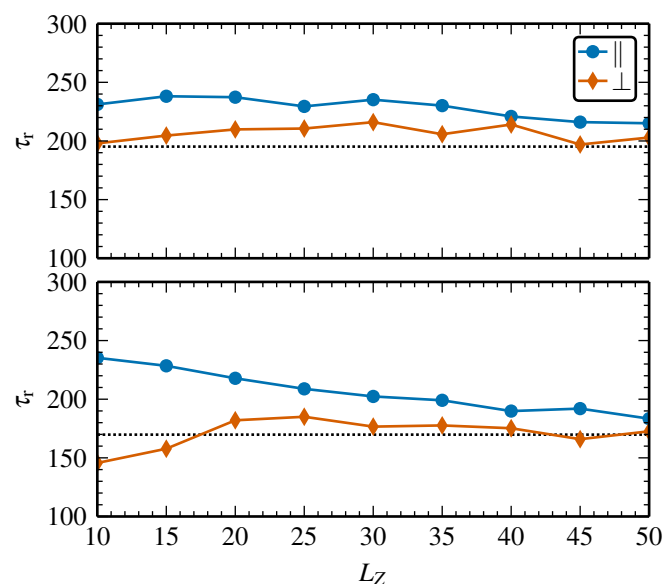


Fig. 8 Relaxation times, τ_r , of one-dimensional orientation autocorrelation function parallel (\parallel) and perpendicular (\perp) to the walls versus distance of walls, L_Z , for an inactive dimer (top) and a sphere-dimer motor (bottom). The dotted horizontal line indicates τ_r for a bulk dimer.

dimer motor exhibits an enhanced diffusive regime and is approximated well by the equation

$$\Delta L^2(t) = 6D_{\text{mt}} - 2\langle V_z \rangle^2 \tau_r^2 \left(1 - e^{-t/\tau_r}\right) - 6 \frac{k_B T}{M_m} \tau_v^2 \left(1 - e^{-t/\tau_v}\right). \quad (1)$$

Here τ_v is the decay time of the velocity fluctuations as determined from the diffusion coefficient of an inactive dimer, $D_0 = (k_B T/M_m) \tau_v$. The MSD reduces to $\Delta L^2(t) \approx (3k_B T/M_m + \langle V_z \rangle^2) t^2$ in the ballistic regime, $t \ll \tau_v$, and to $\Delta L^2(t) \approx 6((k_B T/M_m) \tau_v + \frac{1}{3} \langle V_z \rangle^2 \tau_r) t = 6D_{\text{mt}}$ in the diffusive regime, $t \gg \tau_r$.³³

The MSDs of a confined inactive dimer and a confined sphere-dimer motor are shown in Fig. 9. To account for the confined geometry, the MSDs are separated into components perpendicular and parallel to the walls, $\Delta L_{\perp}(t) = \langle (R_{\perp}(t) - R_{\perp})^2 \rangle$ and $\Delta L_{\parallel}(t) = \frac{1}{2} \langle |\mathbf{R}_{\parallel}(t) - \mathbf{R}_{\parallel}|^2 \rangle$, where $\mathbf{R}(t)$ is the center of mass of the dimer. For both the inactive dimer and the sphere-dimer motor, the parallel components show no dependence on L_Z and overlap exactly with the one-dimensional MSD of the respective bulk case. In contrast, the perpendicular components show L_Z -dependent behaviour. In the inactive case, the perpendicular MSDs reach a diffusive regime for intermediate times for all but the smallest $L_Z = 10$; the diffusion coefficient D_0 decreases with decreasing L_Z . In the mo-

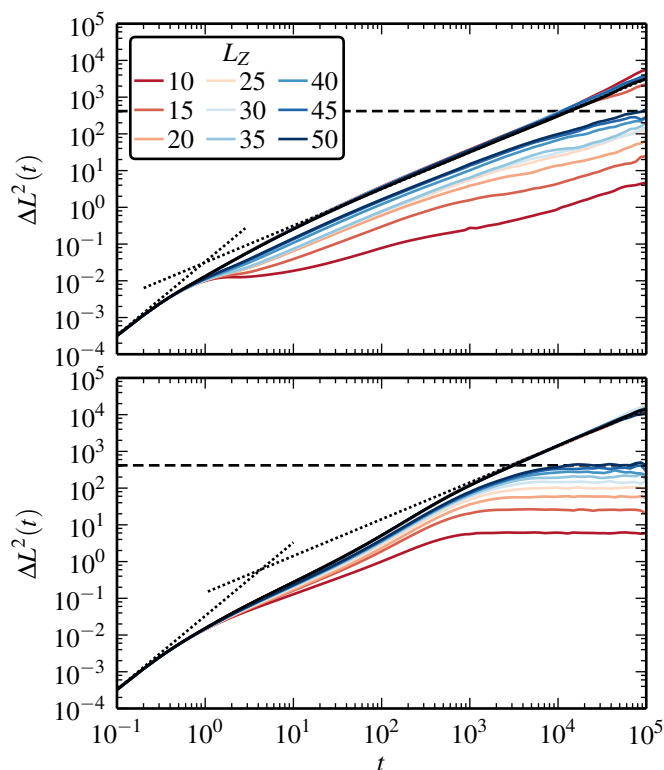


Fig. 9 One-dimensional mean square displacements parallel and perpendicular to walls depending on wall-wall distance L_z , for an inactive dimer (top) and a sphere-dimer motor (bottom). In each panel, the ensemble of overlapping curves at the top corresponds to the parallel MSDs, and the diverging curves below correspond to the perpendicular MSDs. The dashed, horizontal line indicates the theoretical limit of confined diffusion for $L_z = 50$. The dotted lines show the ballistic and diffusive regimes of the one-dimensional MSDs for a bulk dimer.

tor case, the perpendicular MSDs show the same qualitative behaviour as the bulk MSD in the intermediate time regime; however, in the long-time limit, where the bulk MSD reaches the enhanced diffusive regime, the confined MSDs instead converge to L_z -dependent limits, which are in good agreement with the theoretical limit $\frac{1}{6}\Delta L_z^2$ of confined diffusion for a one-dimensional random walk.⁴¹

5 Conclusion

Molecular motors effect active transport in the cell and carry out a variety of other cellular functions. It is certainly interesting to imagine that, in the future, synthetic molecular-scale motors and machines could also be used for biological functions at the cellular level. The fact that the dynamical properties of small catalysts and single enzyme molecules are mod-

ified by chemical activity supports such a notion.^{28–30} While the potential applications of micron-scale motors are being actively explored and many of their properties can be modeled through continuum theories, the dynamics of Ångström-size synthetic motors involve some additional considerations that can only be captured through full molecular dynamics simulations. They are dominated by fluctuations, molecular reorientation often occurs on picosecond time scales limiting the regime where ballistic motion dominates, solvent sizes are often comparable to those of the motor so structural effects come into play and solvent exclusion forces are very strong. These features, combined with the fact that the utility of a continuum description of the solvent velocity flow fields must be confirmed, make these active objects challenging to study.

The results presented in this paper show how these new features, in combination with confinement, change motor spatial structure and dynamics. We have seen that self-propulsion is able to counteract solvent exclusion forces in some circumstances so that the structural ordering of inactive dimers between the walls is very different from that of active dimer motors. The strong anisotropy and spatial dependence of dynamical properties including motor velocity, orientation and diffusion have their origin in the confining geometry. Such information should prove useful for applications involving very small motors in cellular or microfluidic environments.

Acknowledgments

This work was supported in part by a grant from the Natural Sciences and Engineering Research Council of Canada and Compute Canada.

References

- 1 J. Wang, *Nanomachines: Fundamentals and Applications*, Wiley-VCH, Weinheim, 2013.
- 2 R. A. L. Jones, *Soft Machines: Nanotechnology and Life*, Oxford University Press, Oxford, 2004.
- 3 G. A. Ozin, I. Manners, S. Fournier-Bidoz and A. Arsenault, *Adv. Mater.*, 2005, **17**, 3011.
- 4 Y. Hong, D. Velegol, N. Chaturvedi and A. Sen, *Phys. Chem. Chem. Phys.*, 2010, **12**, 1423–1435.
- 5 J. L. Anderson and D. C. Prieve, *Sep. Pur. Reviews*, 1984, **13**, 67–103.
- 6 J. L. Anderson, *Ann. Rev. Fluid Mech.*, 1989, **21**, 61–99.
- 7 R. Golestanian, T. B. Liverpool and A. Ajdari, *Phys. Rev. Lett.*, 2005, **94**, 220801.
- 8 R. Kapral, *J. Chem. Phys.*, 2013, **138**, 020901.
- 9 M. García, J. Orozco, M. Guix, W. Gao, S. Sattayasamitsathit, A. Escarpa, A. Merkoçi and J. Wang, *Nanoscale*, 2013, **5**, 1325.
- 10 S. S. D. Patra, W. Duan, H. Zhang, R. Pavlick and A. Sen, *Nanoscale*, 2013, **5**, 1273.
- 11 W. Gao and J. Wang, *Nanoscale*, 2014, **6**, 10486.
- 12 J. Palacci, C. Cottin-Bizonne, C. Ybert and L. Bocquet, *Phys. Rev. Lett.*, 2010, **105**, 088304.

- 13 I. Theurkauff, C. Cottin-Bizonne, J. Palacci, C. Ybert and L. Bocquet, *Phys. Rev. Lett.*, 2012, **108**, 268303.
- 14 L. F. Valadares, Y.-G. Tao, N. S. Zacharia, V. Kitaev, F. Galembeck, R. Kapral and G. A. Ozin, *Small*, 2010, **6**, 565.
- 15 S. Sengupta, D. Patra, I. Ortiz-Rivera, A. Agrawal, S. Shklyae, K. K. Dey, U. Córdoba-Figueroa, T. E. Mallouk and A. Sen, *Nature Chem.*, 2014, **6**, 415–422.
- 16 M. N. Popescu, S. Dietrich and G. Oshanin, *J. Chem. Phys.*, 2009, **130**, 194702.
- 17 G. Volpe, I. Buttinoni, D. Vogt, H.-J. Kümmerer and C. Bechinger, *Soft Matter*, 2011, **7**, 8810–8815.
- 18 W. E. Uspal, M. N. Popescu, S. Dietrich and M. Tasinkevych, *Soft Matter*, 2014.
- 19 D. G. Crowdy, *J. Fluid Mech.*, 2013, **735**, 473.
- 20 P. Ghosh, V. Misko, F. Marchesoni and F. Nori, *Phys. Rev. Lett.*, 2013, **110**, 268301.
- 21 P. K. Ghosh, *J. Chem. Phys.*, 2014, **141**, 061102.
- 22 J. Elgeti and G. Gompper, *EPL*, 2013, **101**, 48003.
- 23 E. Lauga and T. R. Powers, *Rep. Prog. Phys.*, 2009, **72**, 096601.
- 24 S. E. Spagnolie and E. Lauga, *J. Fluid Mech.*, 2012, **700**, 105.
- 25 J. P. Hernandez-Ortiz, C. G. Stoltz and M. D. Graham, *Phys. Rev. Lett.*, 2005, **95**, 204501.
- 26 J. P. Hernandez-Ortiz, P. T. Underhill and M. D. Graham, *J. Phys.: Condens. Matter*, 2009, **21**, 204107.
- 27 A. Zöttl and H. Stark, *Phys. Rev. Lett.*, 2014, **112**, 118101.
- 28 R. A. Pavlick, K. K. Dey, A. Sirjoosingh, A. Benesi and A. Sen, *Nanoscale*, 2013, **5**, 1301–1304.
- 29 H. S. Muddana, S. Sengupta, T. E. Mallouk, A. Sen and P. J. Butler, *J. Am. Chem. Soc.*, 2010, **132**, 2110–2111.
- 30 S. Sengupta, K. K. Dey, H. S. Muddana, T. Tabouillot, M. E. Ibele, P. J. Butler and A. Sen, *J. Am. Chem. Soc.*, 2013, **135**, 1406–1414.
- 31 T.-C. Lee, M. Alarcón-Correa, C. Miksch, K. Hahn, J. G. Gibbs and P. Fischer, *Nano Lett.*, 2014, **14**, 2407–2412.
- 32 S. Gáspár, *Nanoscale*, 2014, **6**, 7757.
- 33 P. H. Colberg and R. Kapral, *EPL*, 2014, **106**, 30004.
- 34 G. Rückner and R. Kapral, *Phys. Rev. Lett.*, 2007, **98**, 150603.
- 35 Y.-G. Tao and R. Kapral, *J. Chem. Phys.*, 2008, **128**, 164518.
- 36 P. H. Colberg, S. Y. Reigh, B. Robertson and R. Kapral, *Acc. Chem. Res.*, 2014, **47**, 3504.
- 37 The simulations were performed on GPUs and CPUs using a self-written code in the programming languages OpenCL C and Lua.
- 38 A. Rahman, *Phys. Rev.*, 1964, **136**, A405–A411.
- 39 M. N. Popescu, M. Tasinkevych and S. Dietrich, *EPL*, 2011, **95**, 28004.
- 40 S. Y. Reigh and R. Kapral, *Catalytic dimer nanomotors: continuum theory and microscopic dynamics*, Submitted.
- 41 T. Bickel, *Physica A*, 2007, **377**, 24–32.